


Article

Effects of Strain Rate and Measuring Temperature on the Elastocaloric Cooling in a Columnar-Grained $\text{Cu}_{71}\text{Al}_{17.5}\text{Mn}_{11.5}$ Shape Memory Alloy

Hui Wang, Haiyou Huang *  and Jianxin Xie

Key Laboratory for Advanced Materials Processing of the Ministry of Education, Institute for Advanced Materials and Technology, University of Science and Technology Beijing, Beijing 100083, China; wangh9130@163.com (H.W.); jxxie@ustb.edu.cn (J.X.)

* Correspondence: huanghy@mater.ustb.edu.cn; Tel.: +86-010-6233-2253

Received: 22 October 2017; Accepted: 18 November 2017; Published: 27 November 2017

Abstract: Solid-state refrigeration technology based on elastocaloric effects (eCEs) is attracting more and more attention from scientists and engineers. The response speed of the elastocaloric materials, which relates to the sensitivity to the strain rate and measuring temperature, is a significant parameter to evaluate the development of the elastocaloric material in device applications. Because the Cu-Al-Mn shape memory alloy (SMA) possesses a good eCE and a wide temperature window, it has been reported to be the most promising elastocaloric cooling material. In the present paper, the temperature changes (ΔT) induced by reversible martensitic transformation in a columnar-grained $\text{Cu}_{71}\text{Al}_{17.5}\text{Mn}_{11.5}$ SMA fabricated by directional solidification were directly measured over the strain rate range of $0.005\text{--}0.19\text{ s}^{-1}$ and the measuring temperature range of $291\text{--}420\text{ K}$. The maximum adiabatic ΔT of 16.5 K and a lower strain-rate sensitivity compared to TiNi-based SMAs were observed. With increasing strain rate, the ΔT value and the corresponding coefficient of performance (COP) of the alloy first increased, then achieved saturation when the strain rate reached 0.05 s^{-1} . When the measuring temperature rose, the ΔT value increased linearly while the COP decreased linearly. The results of our work provide theoretical reference for the design of elastocaloric cooling devices made of this alloy.

Keywords: shape memory alloy; columnar grain; Cu-Al-Mn; elastocaloric effect; strain rate; measuring temperature

1. Introduction

The elastocaloric effect (eCE) refers to the thermal response of a given material to external uniaxial stress, which is commonly quantified by the isothermal entropy change (ΔS) and adiabatic temperature change (ΔT). Elastocaloric refrigeration based on eCEs, which is a new type of solid-state refrigeration, has drawn significant attention in recent years owing to its higher coefficient of performance (COP), its lower device costs, and its eco-friendliness as a promising alternative to conventional vapor compression, as well as to its downscaling ability for microcooling [1–5]; it is regarded as the most applicable solid-state refrigeration technology [6]. Shape memory alloys (SMAs) can undergo a reversible martensitic transformation (MT) by applying external stress, which is accompanied by a large latent heat absorption and release. These features make them important elastocaloric materials and thus draw momentous attention.

The refrigeration capability (RC) of a given elastocaloric material can be evaluated by directly measuring the adiabatic temperature change of the phase transformation or deformation. Some related research indicated that a high ΔT value of more than 10 K has been directly measured in Ti-Ni- [7,8], Ni-Fe- [9] and Cu-based SMAs [10], which has laid a good material foundation for the

development and application of elastocaloric refrigeration technology. At present, an increasing number of promising elastocaloric refrigeration devices are being developed [11]. In addition to evaluating the RC, the responding speed of SMAs is also a significant factor that influences the system cooling efficiency of the solid refrigeration system. Some researchers have carried out a series of research on the influence of strain rates on the eCE in Ti-Ni-based SMAs, such as $\text{Ti}_{49.1}\text{Ni}_{50.5}\text{Fe}_{0.4}$ foils and $\text{Ti}_{50.4}\text{Ni}_{49.6}$ films by Ossmer et al. [12,13], $\text{Ti}_{51.1}\text{Ni}_{48.9}$ wires by Tušek et al. [8], $\text{Ti}_{55.4}\text{Ni}_{44.6}$ wires by Tobush et al. [14], a $\text{Ti}_{47.25}\text{Ni}_{45}\text{Cu}_5\text{V}_{2.75}$ block by Schmidt et al. [15], and so on. Compared with the Ti-Ni-based SMAs, Cu-based SMAs also have a large ΔT value, which has been proved by Xu et al. They found a ΔT value of 12–13 K in columnar-grained Cu-Al-Mn SMAs [10], covering a wide temperature range of more than 100 K, which, combined with a low applying stress [10,16] and low material costs, make the columnar-grained Cu-Al-Mn SMAs a promising material for solid-state refrigeration. In this paper, over the strain rate from 0.005 to 0.19 s^{-1} and the test temperature range from 291 to 393 K, the temperature changes induced by reversible MT of columnar-grained $\text{Cu}_{71}\text{Al}_{17.5}\text{Mn}_{11.5}$ SMAs have been systematically measured, the effects of the strain rate ($\dot{\epsilon}$) and measuring temperature (T_A) on the eCEs have been obtained, and the influence mechanism is discussed. The results of this study can provide a theoretical reference for the design and application of elastocaloric cooling devices that are made of Cu-based SMAs.

2. Materials and Methods

A $\text{Cu}_{71}\text{Al}_{17.5}\text{Mn}_{11.5}$ ingot with a columnar-grained microstructure was prepared by directional solidification [17]. At first, the ingot was annealed at 1073 K for 5 min followed by quenching into ice water to obtain a single β_1 phase. Then, the ingot was aged at 473 K for 15 min to stabilize the MT temperatures. Dog bone-shaped tensile samples with a gauge size of 25 mm \times 6 mm \times 2 mm were cut out from the ingot, with their longitudinal direction along the solidification direction (SD). The surface of the tensile specimen was polished with 500–3000 # sandpaper and then subjected to mechanical polishing and electrolytic polishing. The texture characterization was conducted by electron back-scattered diffraction (EBSD) with a minimum misorientation resolution of 2°. The electrolytic polishing solution was as follows: 250 mL of H_3PO_4 , 250 mL of alcohol, 50 mL of glycerol, 5 g of urea, and 500 mL of H_2O , with a voltage of 10 V and duration from 80 to 120 s. The transformation temperatures and latent heat were determined by NETZSCH 404F3 using differential scanning calorimetry (DSC, Mettler-Toledo, Zurich, Switzerland) under a nitrogen inert gas flow of 10 $\text{mL}\cdot\text{s}^{-1}$ with a heating/cooling rate of 10 K/min. Tensile tests were conducted on a Mechanical Testing System (MTS) testing machine (Wister Industrial Equipment cooperation Limited, Shenzhen, China) equipped with a thermostatic chamber. During the tensile test, all samples were loaded at a constant strain rate of 0.05 s^{-1} to the maximum strain of 10% and were then unloaded at different strain rates to zero stress. In this work, the measuring temperature range was from 291 to 420 K, and the unloading strain rate range was from 0.005 to 0.19 s^{-1} . The temperature of the sample in the tensile cycle was monitored with a K-type thermocouple welded on the center of the sample surface. The authors used a set of self-built equipment for data acquisition and a MATLAB program (v7.0, MathWorks, Natick, MA, USA, 2012) to display the measured temperature.

3. Results and Discussion

The $\text{Cu}_{71}\text{Al}_{17.5}\text{Mn}_{11.5}$ SMA sample was composed of a single austenite phase β_1 with L2₁ crystallographic structure at room temperature. When a stress applied in the sample was higher than the critical stress of MT, a stress-induced MT of $\beta_1 \rightarrow \beta_1'$ occurred and the β_1' martensite had an 18R ordered structure. The phase structure and transformation behavior have been determined by X-ray diffraction (XRD, SmartLab, Rigaku Corporation, Matsubara-cho, Akishima-shi, Tokyo, Japan) and transmission electron microscopy (TEM, F20, FEI, Hillsboro, OR, USA) operated at 200 kV at room temperature in previous work by authors and other researchers [18–22].

The DSC curve during the heating/cooling process of the as-quenched sample is shown in Figure 1. An exothermic peak corresponding to the MT during cooling and an endothermic peak corresponding to the reverse austenitic transformation during heating can be clearly observed. The MT and reverse transformation temperatures can be obtained from the curve: the MT starting temperature was $M_s = 247$ K, the MT finishing temperature was $M_f = 235$ K, the reverse transformation starting temperature was $A_s = 253$ K and the reverse transformation finishing temperature was $A_f = 265$ K; the thermal hysteresis was 18 K.

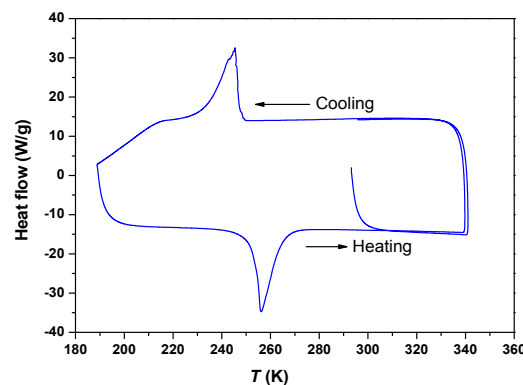


Figure 1. Differential scanning calorimetry (DSC) curve of the columnar-grained $\text{Cu}_{71}\text{Al}_{17.5}\text{Mn}_{11.5}$ shape memory alloy (SMA; heating/cooling rate of 10 K/min).

The EBSD orientation map and the inverse pole figures (Figure 2) illustrate that the columnar-grained Cu-Al-Mn sample has a strong $\langle 001 \rangle$ oriented texture along the SD (solidification direction).

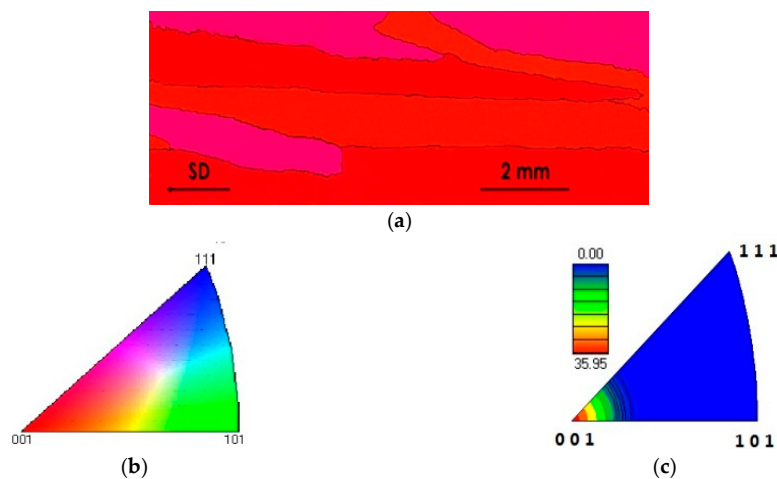


Figure 2. (a) Electron back-scattered diffraction (EBSD) quasi-colored orientation map along solidification direction (SD); (b) the reference stereographic triangle; (c) inverse pole figure along the SD, which illustrate that the columnar-grained $\text{Cu}_{71}\text{Al}_{17.5}\text{Mn}_{11.5}$ SMA sample has a strong $\langle 001 \rangle$ -oriented texture along the SD.

The tensile stress-strain curves for the columnar-grained $\text{Cu}_{71}\text{Al}_{17.5}\text{Mn}_{11.5}$ SMA are shown in Figure 3; these were tested at the same loading strain rate $\dot{\epsilon}_l$ of 0.05 s^{-1} while gradually increasing the unloading strain rates $\dot{\epsilon}_u$ from 0.005 to 0.19 s^{-1} . Specifically, nine strain rates of 0.005 , 0.01 , 0.05 , 0.07 , 0.096 , 0.1 , 0.13 , 0.15 , and 0.19 s^{-1} were chosen. It should be noted that in order to avoid the experimental deviation from different samples, the test was carried out using the same sample at each measuring temperature. For all the test conditions in Figure 3, when the measuring temperature was ≤ 393 K, an almost 100% strain

recovery could be observed after the samples underwent a loading strain of 10%, indicating an excellent superelasticity of the columnar-grained $\text{Cu}_{71}\text{Al}_{17.5}\text{Mn}_{11.5}$ SMA. With increasing tensile cycles, both the critical stresses of MT and reverse transformation were decreased gradually. Because the loading strain rate is constant, the stress of MT decreasing in loading processes can be attributed to the influence of cycle numbers, which may be related to the fatigue effect. However, the stress of reverse transformation in unloading processes may be affected by loading processes, strain rates or cycle numbers.

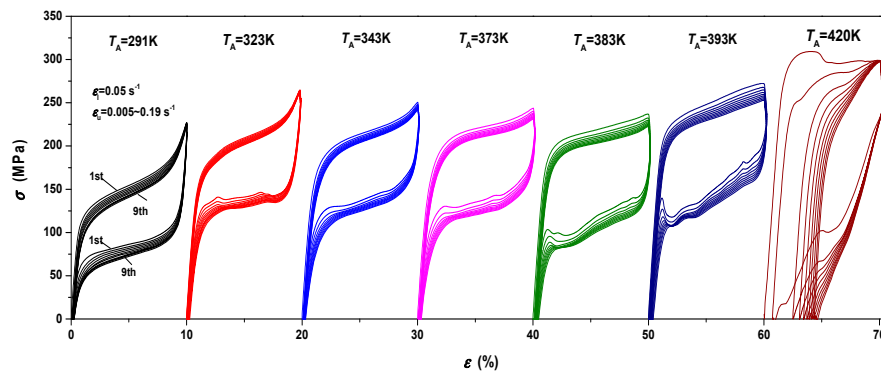


Figure 3. Stress-strain curves for the columnar-grained $\text{Cu}_{71}\text{Al}_{17.5}\text{Mn}_{11.5}$ shape memory alloys (SMAs) with different unloading strain rates ($\dot{\epsilon}_u = 0.005\text{--}0.19 \text{ s}^{-1}$) at different measuring temperatures.

In this work, the influence of loading processes can be excluded as a result of the same loading strain and loading strain rate. In order to clarify the influence of cycle numbers or strain rate on the unloading curves, a comparative tensile test with 10 cycles was carried on at a constant unloading rate of 0.05 s^{-1} , and the stress-strain curves are shown in Figure 4a. Comparing the stress-strain curve tested at 291 K in Figure 3 and the curve in Figure 4a, the reduction of the transformation stress has closed relations with the increase in cycle numbers. In other words, the strain rate has little effect on the transformation stress of columnar-grained $\text{Cu}_{71}\text{Al}_{17.5}\text{Mn}_{11.5}$ SMA, which is different from the phenomenon that was observed in Ti-Ni alloys [14,15]. For Ti-Ni alloys, with increasing strain rates, the stress-strain loop enlarges clearly; that is, the loading stress increases and unloading stress decreases. The strain rate sensitivity of the transformation stress in SMAs is related to the capability of stress relaxation, which is caused by martensite nucleation and growth during the MT process. Under constant strain conditions, the MT of Ti-Ni SMAs requires 3 min to induce a stress relaxation of 50 MPa [15]. In other words, when the strain rate exceeds 0.02 s^{-1} of Ti-Ni SMAs, the stress will clearly increase as a result of stress relaxation hysteresis. Figures 3 and 4a indicate that the phenomenon of transformation stress increase is not observed in columnar-grained $\text{Cu}_{71}\text{Al}_{17.5}\text{Mn}_{11.5}$ SMAs until the strain rate reaches 0.19 s^{-1} , which means that the stress relaxation capacity of columnar-grained $\text{Cu}_{71}\text{Al}_{17.5}\text{Mn}_{11.5}$ SMAs is more than 10 times that of Ti-Ni SMAs. Therefore, the strain rate sensitivity of columnar-grained $\text{Cu}_{71}\text{Al}_{17.5}\text{Mn}_{11.5}$ SMAs is dramatically lower than that of Ti-Ni SMAs.

In order to study the effect of measuring temperature on tensile stress-strain curves of the columnar-grained $\text{Cu}_{71}\text{Al}_{17.5}\text{Mn}_{11.5}$ SMA, a series of tensile cycle tests were carried out between the temperature range from 291 to 420 K, and the results are subsequently drawn in Figure 3. A comparison of these stress-strain curves indicates that as the measuring temperature rises, the MT stress increases gradually. When the measuring temperature reaches 420 K, the recoverable strain of the sample decreases rapidly with the increase in the number of tensile cycles. The microstructure observation found that a large number of dislocations were observed in the sample, indicating that the tensile stress was high enough to start the dislocation slip. This phenomenon implies the deformation mechanism begins to change from superelastic deformation induced by phase transformation to permanent plastic deformation caused by a dislocation slip when the sample deforms at 420 K, which can be defined as the critical temperature of stress-induced MT in columnar-grained $\text{Cu}_{71}\text{Al}_{17.5}\text{Mn}_{11.5}$ alloys. Therefore,

the upper limit of the temperature window of the eCE of columnar-grained $\text{Cu}_{71}\text{Al}_{17.5}\text{Mn}_{11.5}$ alloys is less than 420 K. In other words, the temperature window of the columnar-grained $\text{Cu}_{71}\text{Al}_{17.5}\text{Mn}_{11.5}$ alloy is 265–393 K. The width of the temperature window is 128 K.

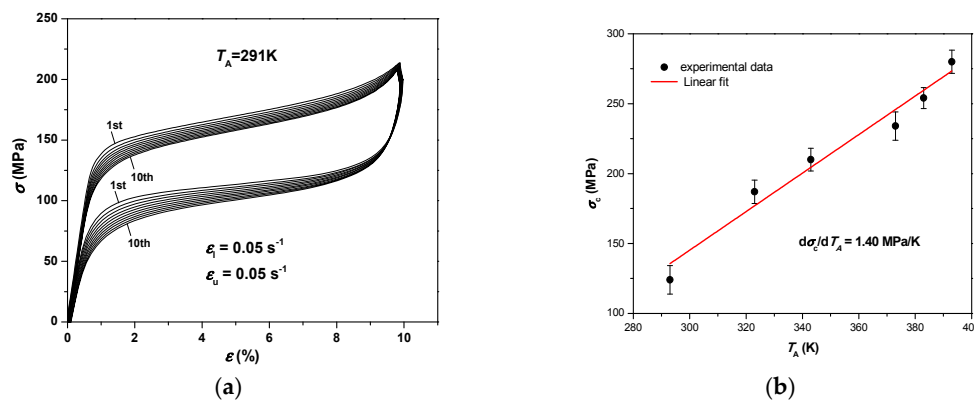


Figure 4. (a) Stress-strain curves with constant loading rate ($\dot{\epsilon}_l = 0.05\text{ s}^{-1}$) at 291 K; (b) T_A dependence of σ_c for the columnar-grained $\text{Cu}_{71}\text{Al}_{17.5}\text{Mn}_{11.5}$ shape memory alloy (SMA).

On the basis of the first cycle of the measured stress–strain curve in the temperature range of 291–393 K, the MT critical stress (σ_c) as a function of T_A is plotted in Figure 4b. Figure 4b indicates that σ_c linearly increases with the increase of measuring temperature in the range of 291–393 K, and $d\sigma_c/dT_A = 1.40\text{ MPa/K}$ for the columnar-grained $\text{Cu}_{71}\text{Al}_{17.5}\text{Mn}_{11.5}$ alloy, which can be determined by linear fitting.

Figure 5 indicates the temperature change of the columnar-grained $\text{Cu}_{71}\text{Al}_{17.5}\text{Mn}_{11.5}$ SMA samples in loading-unloading cycles at different measuring temperatures. It can be seen from Figure 5a–d that at a constant strain rate (0.05 s^{-1}), the ΔT values measured from both loading and unloading processes for different cycles are almost unchanged in the temperature range of 291–393 K, which indicates that no evident influence of cycle numbers on ΔT was observed after 10 tensile cycles at a constant strain rate; this implies a good stability of the eCE in the columnar-grained $\text{Cu}_{71}\text{Al}_{17.5}\text{Mn}_{11.5}$ SMA. When the strain rate is less than 0.05 s^{-1} , $|\Delta T|$ increases with increasing $\dot{\epsilon}_u$. When the strain rate reaches 0.05 s^{-1} or above, $|\Delta T|$ achieves saturation. For instance, at $T_A = 291\text{ K}$, when $\dot{\epsilon}_u$ increases from 0.005 to 0.05 s^{-1} , ΔT changes from 7.53 to 11.21 K. After $\dot{\epsilon}_u$ reaches 0.05 s^{-1} , the ΔT values remain constant within the range of 11.21–11.51 K. For different T_A values, the variation trends of the T vs. t curves from the samples with increasing $\dot{\epsilon}_u$ are similar.

In addition, the phenomenon of temperature irreversibility can also be found from Figure 5; that is, the absolute values of the temperature change between loading and unloading are not equal. For example, when the strain rate is 0.05 s^{-1} at 291 K, the loading temperature rises are 14.8–15.3 K (Figure 5a) and 13.7–13.9 K (Figure 5b), while the unloading temperature drops are 13.2–13.5 K (Figure 3a) and 11.2 K (Figure 5b). The absolute value of the unloading temperature drop is 1.6–2.7 K, which is lower than the loading temperature rise. Irreversibility is caused by the existence of the hysteresis area during the loading-unloading process. The formation of the hysteresis area is directly related to the frictional origin during the transformation. These frictions include the interfacial friction between martensite and austenite, the interaction between the phase interface and grain boundary, or other defects [12,14]. When the measuring temperature reached 420 K, as a result of the occurrence of irreversible deformation caused by a dislocation slip, the return strain gradually reduced with the increasing stretching cycles, resulting in a gradually reduced temperature change, as shown in Figure 5e.

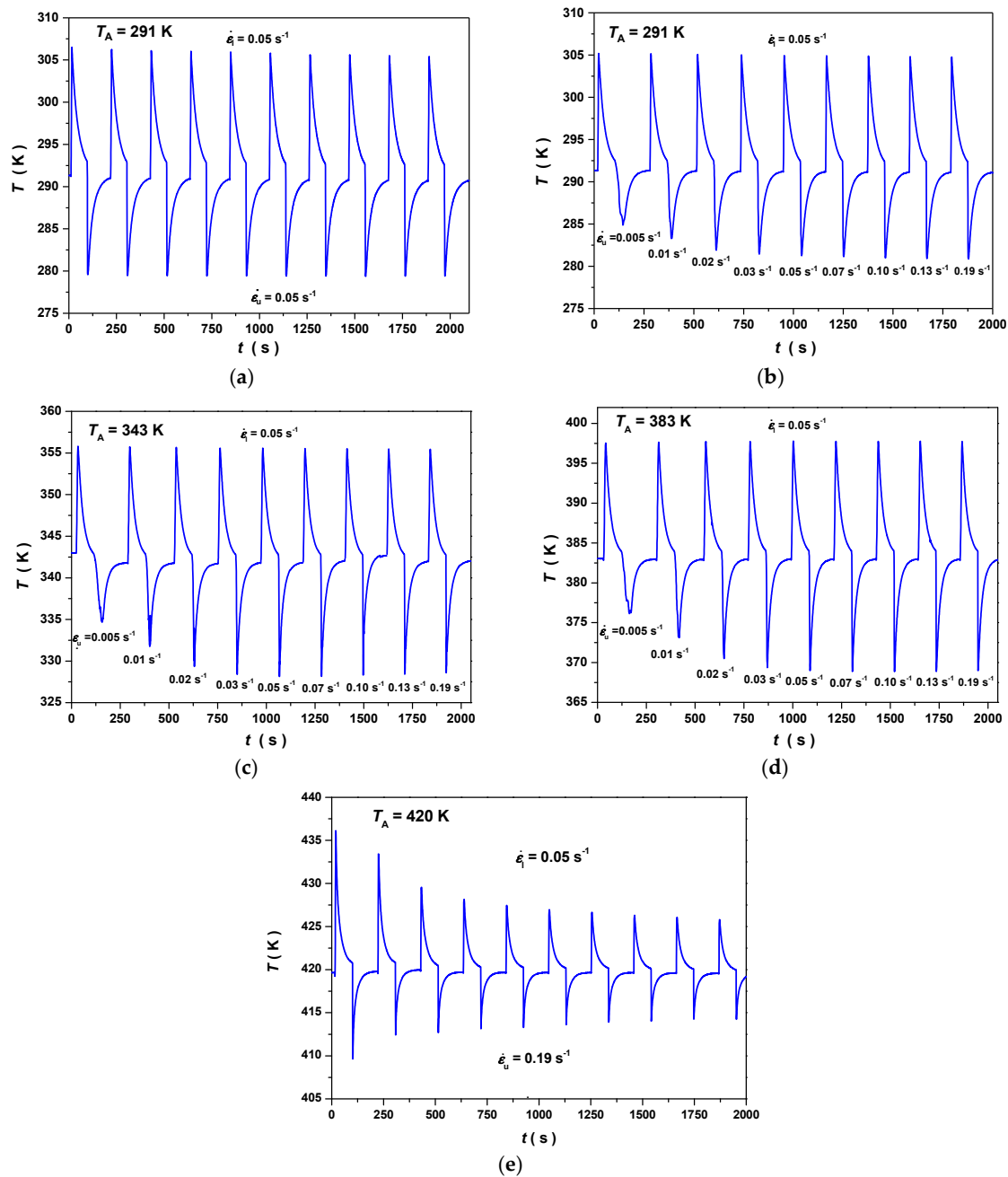


Figure 5. Temperature-time profiles with a specific unloading strain rate: (a) $\dot{\epsilon}_u = 0.05 \text{ s}^{-1}$, $T_A = 291 \text{ K}$; (e) $\dot{\epsilon}_u = 0.19 \text{ s}^{-1}$, $T_A = 420 \text{ K}$ and with various unloading strain rates ($\dot{\epsilon}_u = 0.005\text{--}0.19 \text{ s}^{-1}$) at $T_A = 291 \text{ K}$ (b); $T_A = 343 \text{ K}$ (c); and $T_A = 383 \text{ K}$ (d) for the columnar-grained $\text{Cu}_{71}\text{Al}_{17.5}\text{Mn}_{11.5}$ shape memory alloy (SMA) samples ($\dot{\epsilon}_l = 0.05 \text{ s}^{-1}$ for all samples).

On the basis of the T - t profiles (four typical profiles are shown in Figure 5), a high $|\Delta T|$ value of 11.3–16.5 K can be obtained in the columnar-grained $\text{Cu}_{71}\text{Al}_{17.5}\text{Mn}_{11.5}$ SMA during unloading processes, covering a wide temperature range of more than 100 K. The entropy change of the phase transformation associated with the elastocaloric cooling can be estimated as

$$\Delta S \approx -\frac{\Delta T}{T_A} C_p \quad (1)$$

where C_p is the heat capacity, measured to be 455 J/kg·K for the $\text{Cu}_{71}\text{Al}_{17.5}\text{Mn}_{11}$ SMA [10]. Strictly speaking, when calculating the adiabatic temperature change or entropy change, because of the coexistence of two phases during transformation, we should consider that $C_p = xC_p^A + (1 - x)C_p^M$, where x is the fraction of the authentic phase, and C_p^A and C_p^M are the heat capacity of the authentic phase and martensitic phase, respectively. However, C_p^A and C_p^M are approximately equal for SMAs [23]. Therefore, in the actual measurement and calculation, we supposed $C_p \approx C_p^A \approx C_p^M$. In this paper, we experimentally measured the C_p^A value and used it in the calculation. According to the ΔT values measured above, the maximum ΔS can be estimated to be 19.5 J/(kg·K). Additionally, ΔS can also be calculated from the Clausius-Clapeyron equation:

$$\Delta S = -\frac{1}{\rho} \frac{d\sigma_c}{dT_A} \varepsilon \quad (2)$$

where ρ is the density and ε is the transformation strain. For the columnar-grained $\text{Cu}_{71}\text{Al}_{17.5}\text{Mn}_{11.5}$ SMA, $d\sigma_c/dT_A$ and ε can be determined to be 1.40 MPa/K from Figure 4b and 8.3% from Figure 3, and $\rho = 7.40 \times 10^3 \text{ kg/m}^3$ [24]. The calculated ΔS value from the Clausius-Clapeyron equation is about 15.7 J/(kg·K), which is smaller than the calculation results based on ΔT . In addition, the theoretical maximum of the isothermal entropy change also can be calculated to be 25.0 J/kg·K by the latent heat of phase transformation determined by DSC measurement [10]. Therefore, the entropy change estimated on the basis of the experimental data in this paper approached ~78% of its theoretical value. It is generally believed that the latent heat of phase transformation determined by the DSC method corresponds to a completed entropy change from 100% phase transformation without any loss, thus often called the theoretical entropy change. The entropy change value estimated on the basis of the experimentally measured ΔT value is less than the theoretical entropy change, because of the existence of internal frictions induced by the phase interface frictions and the interactions between phase migration and defects. In addition, in the actual tensile deformation processes, incomplete MT may be another probable cause of the smaller entropy change value estimated by stress-strain curves. According to the above discussion, the energy loss induced by internal frictions is about 5.5 J/(kg·K) for the columnar-grained $\text{Cu}_{71}\text{Al}_{17.5}\text{Mn}_{11.5}$ SMA.

The $|\Delta T|$ value and the COP for unloading processes in the columnar-grained $\text{Cu}_{71}\text{Al}_{17.5}\text{Mn}_{11.5}$ SMA as a function of $\dot{\varepsilon}$ and T_A are summarized in Figure 6. The COP of the material, which describes the cooling efficiency, is defined by the ratio of cooling power (ΔQ) to input work (ΔW) [25]:

$$\text{COP} = \Delta Q / \Delta W \quad (3)$$

where ΔQ can be estimated from the latent heat, which is $\Delta T_{ad} \times C_p$ (ΔT_{ad} is the adiabatic temperature change), and ΔW can be obtained by integrating the area enclosed by the stress hysteresis loop (Figure 3). Figure 6a indicates that all $|\Delta T|$ vs. $\dot{\varepsilon}$ curves show a similar variation trend. At first, the $|\Delta T|$ value increases with increasing $\dot{\varepsilon}$. When the strain rate reaches 0.05 s^{-1} , the $|\Delta T|$ value remains almost unchanged, implying it achieves saturation. The critical strain rate $\dot{\varepsilon}_c$ corresponding to the onset of $|\Delta T|$ saturation is less than that of Ti-Ni alloy, which was reported as 0.2 s^{-1} [13]. In other words, it is easier to reach near-adiabatic conditions using the columnar-grained $\text{Cu}_{71}\text{Al}_{17.5}\text{Mn}_{11.5}$ SMA. In the process of MT (reverse MT), the homogeneity of martensite (austenite) nucleation and extension is a noteworthy factor to influence $\dot{\varepsilon}_c$. The more homogeneously the MT occurs in the sample, the lower the $\dot{\varepsilon}_c$ value [12]. The columnar-grained Cu-Al-Mn SMA has a homogeneous contribution of stress/strain in the whole sample as a result of a high deformation and transformation compatibility among grains [26]. Therefore, the martensite (austenite) can nucleate and grow homogeneously in the columnar-grained samples. Furthermore, the Cu-based SMAs have a higher thermal conductivity compared to the Ti-Ni alloy, which also helps to obtain a uniform temperature distribution within a very short period of time. The above two reasons show that the

columnar-grained $\text{Cu}_{71}\text{Al}_{17.5}\text{Mn}_{11.5}$ SMA has a low $\dot{\epsilon}_c$, which can reduce the design difficulty of refrigeration devices.

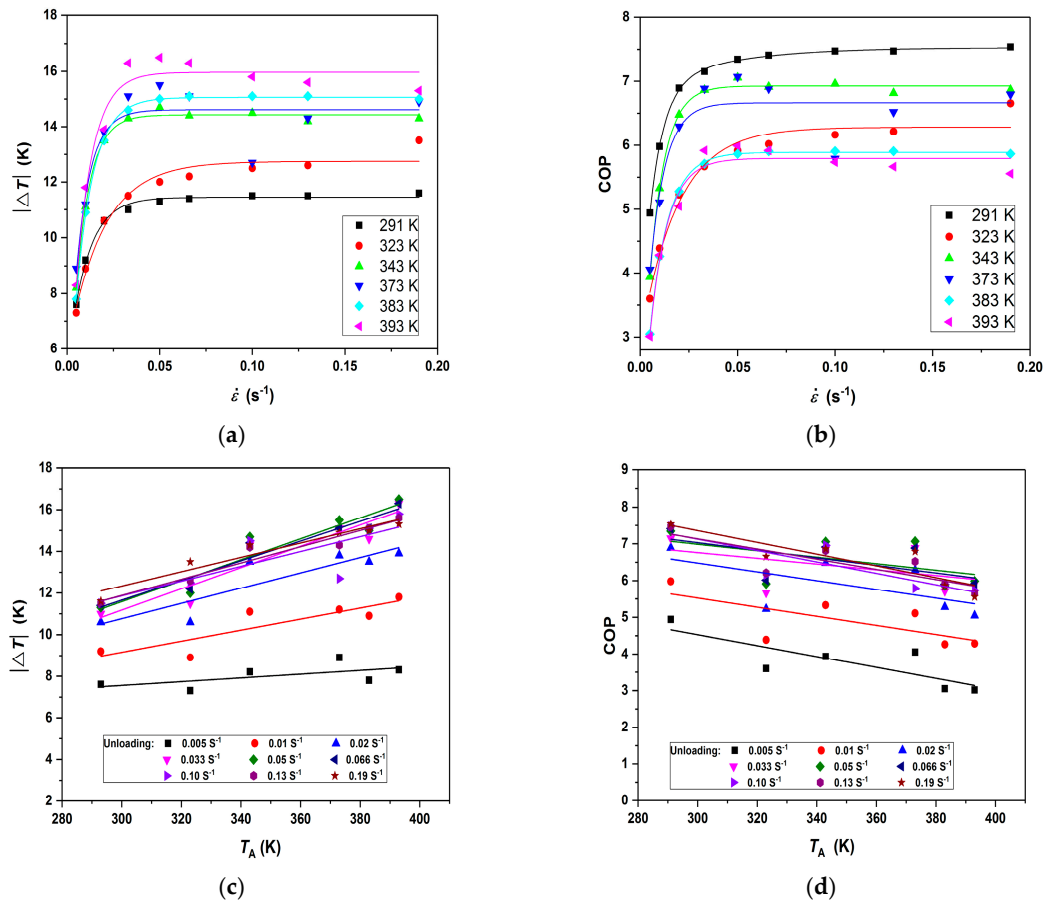


Figure 6. The $|\Delta T|$ and coefficient of performance (COP) values for unloading process in the columnar-grained $\text{Cu}_{71}\text{Al}_{17.5}\text{Mn}_{11.5}$ shape memory alloy (SMA) as a function of $\dot{\epsilon}$ and T_A : (a) $|\Delta T|$ vs. $\dot{\epsilon}$; (b) COP vs. $\dot{\epsilon}$; (c) $|\Delta T|$ vs. T_A ; (d) COP vs. T_A .

Figure 6b indicates that the variation trend of COP with increasing strain rate is consistent with $|\Delta T|$, while the variations of $|\Delta T|$ and COP with T_A are the opposite, as shown in Figure 6c,d. For refrigeration device or system design, a higher $|\Delta T|$ and COP are expected. For the columnar-grained $\text{Cu}_{71}\text{Al}_{17.5}\text{Mn}_{11.5}$ SMA, in order to achieve a stable and high refrigeration capability and COP, the applied strain rates should be more than 0.05 s^{-1} .

4. Conclusions

In summary, the effects of strain rates and the measuring temperature on the elastocaloric cooling in a columnar-grained $\text{Cu}_{71}\text{Al}_{17.5}\text{Mn}_{11.5}$ SMA were experimentally investigated over the strain rate range of $0.005\text{--}0.19 \text{ s}^{-1}$ and the measuring temperature range of $291\text{--}393 \text{ K}$. With the increasing strain rate, the ΔT and COP values of the alloy increase firstly and then achieve saturation when the strain rate reaches 0.05 s^{-1} , which indicates a lower strain rate sensitivity of refrigeration capability compared to Ti-Ni-based SMAs (about 0.2 s^{-1}). The relatively low strain rate sensitivity of the columnar-grained $\text{Cu}_{71}\text{Al}_{17.5}\text{Mn}_{11.5}$ SMA is attributed to two reasons. The first is a high deformation and phase transformation compatibility among grains in the columnar-grained microstructure, which causes a homogenous stress/strain distribution in the entire samples. The other is a high thermal conductivity of Cu-based SMAs, which also helps to obtain a uniform temperature distribution in a very short period of time. In addition, a maximum adiabatic ΔT value of 16.5 K with corresponding

ΔS of 19.5 J/(kg·K) and a wide operational temperature window ($\omega_T > 100$ K) were directly measured in the experiment. The above results demonstrate that the columnar-grained Cu₇₁Al_{17.5}Mn_{11.5} SMA is a promising candidate of elastocaloric materials with the advantages of a high refrigeration capability in a wide strain-rate range and operational temperature window, which are beneficial for the design and application to refrigeration devices.

Acknowledgments: This work was supported by the National Key Research and Development Program of China (Grant No. 2016YFB0700500) and the National Natural Science Foundation of China (Grant No. 51574027). Hui Wang thanks the State Key Laboratory of Technologies in Space Cryogenics Propellants, Technical Institute of Physics and Chemistry, Chinese Academy of Sciences for providing experimental equipment.

Author Contributions: Hui Wang and Haiyou Huang conceived and designed the experiments; Hui Wang performed the experiments; Hui Wang and Haiyou Huang analyzed the data and wrote the paper; Haiyou Huang and Jianxin Xie supported the writing of the paper. All authors participated in the discussions of the results.

Conflicts of Interest: The authors declare no conflict of interest.

References

1. Moya, X.; Kar-Narayan, S.; Mathur, N.D. Caloric materials near ferroic phase transitions. *Nat. Mater.* **2014**, *13*, 439–450. [[CrossRef](#)] [[PubMed](#)]
2. Gschneidner Jr., K.A.; Pecharsky, V.K.; Tsokol, A.O. Recent developments in magnetocaloric materials. *Rep. Prog. Phys.* **2005**, *68*, 1479–1539. [[CrossRef](#)]
3. Mischenko, A.S.; Zhang, Q.; Scott, J.F.; Whatmore, R.W.; Mathur, N.D. Giant electrocaloric effect in thin-film PbZr_{0.95}Ti_{0.05}O₃. *Science* **2006**, *311*, 1270–1271. [[CrossRef](#)] [[PubMed](#)]
4. Mañosa, L.; González-Alonso, D.; Planes, A.; Bonnot, E.; Barrio, M.; Tamarit, J.L.; Aksoy, S.; Acet, M. Giant solid-state barocaloric effect in the Ni-Mn-In magnetic shape-memory alloy. *Nat. Mater.* **2010**, *9*, 478–481. [[CrossRef](#)] [[PubMed](#)]
5. Bonnot, E.; Romero, R.; Mañosa, L.; Vives, E.; Planes, A. Elastocaloric effect associated with the martensitic transition in shape-memory alloys. *Phys. Rev. Lett.* **2008**, *100*, 125901. [[CrossRef](#)] [[PubMed](#)]
6. Goetzler, W.; Zogg, R.; Young, J.; Johnson, C. *Energy Savings Potential and RD&D Opportunities for Non-Vapor-Compression HVAC Technologies*; U.S. Department of Energy (Navigant Consulting Inc.): Washington, DC, USA, 2014.
7. Cui, J.; Wu, Y.; Muehlbauer, J.; Hwang, Y.; Radermacher, R.; Fackler, S.; Wuttig, M.; Takeuchi, I. Demonstration of high efficiency elastocaloric cooling with large ΔT using NiTi wires. *Appl. Phys. Lett.* **2012**, *101*, 1175–1178. [[CrossRef](#)]
8. Tušek, J.; Engelbrecht, K.; Mikkelsen, L.; Pryds, N. Elastocaloric effect of Ni-Ti wire for application in a cooling device. *J. Alloys Compd.* **2015**, *117*, 10–19. [[CrossRef](#)]
9. Pataky, G.J.; Ertekin, E.; Sehitoglu, H. Elastocaloric cooling potential of NiTi, Ni₂FeGa, and CoNiAl. *Acta Mater.* **2015**, *96*, 420–427. [[CrossRef](#)]
10. Xu, S.; Huang, H.Y.; Xie, J.; Takekawa, S.; Xu, X.; Omori, T.; Kainuma, R. Giant elastocaloric effect covering wide temperature range in columnar-grained Cu_{71.5}Al_{17.5}Mn₁₁ shape memory alloy. *APL Mater.* **2016**, *4*, 106106. [[CrossRef](#)]
11. Qian, S.; Geng, Y.; Wang, Y.; Radermacher, R. A review of elastocaloric cooling: Materials, cycles and system integrations. *Int. J. Refrig.* **2016**, *64*, 1–19. [[CrossRef](#)]
12. Ossmer, H.; Miyazaki, S.; Kohl, M. The elastocaloric effect in TiNi-based foils. *Mater. Today Proc.* **2015**, *2*, S971–S974. [[CrossRef](#)]
13. Ossmer, H.; Lambrecht, F.; Gültig, M.; Chluba, C.; Quandt, E.; Kohl, M. Evolution of temperature profiles in Ti-Ni films for elastocaloric cooling. *Acta Mater.* **2014**, *81*, 9–20. [[CrossRef](#)]
14. Tobushi, H.; Shimeno, Y.; Hachisuka, T.; Tanaka, K. Influence of strain rate on superelastic properties of TiNi shape memory alloy. *Mech. Mater.* **1998**, *30*, 141–150. [[CrossRef](#)]
15. Schmidt, M.; Schütze, A.; Seelecke, S. Elastocaloric cooling processes: The influence of material strain and strain rate on efficiency and temperature span. *Appl. Phys. Lett.* **2016**, *4*, 10–19. [[CrossRef](#)]
16. Manosa, L.; Jarque-Farnos, S.; Vives, E.; Planes, A. Large temperature span and giant refrigerant capacity in elastocaloric Cu-Zn-Al shape memory alloys. *Appl. Phys. Lett.* **2013**, *103*, 211904. [[CrossRef](#)]

17. Liu, J.L.; Huang, H.Y.; Xie, J.X. Superelastic anisotropy characteristics of columnar-grained Cu-Al-Mn shape memory alloys and its potential applications. *Mater. Des.* **2015**, *85*, 211–220. [[CrossRef](#)]
18. Xu, S.; Huang, H.; Xie, J.; Kimura, Y.; Xu, X.; Omori, T.; Kainuma, R. Dynamic recovery and superelasticity of columnar-grained Cu-Al-Mn shape memory alloy. *Metals* **2017**, *7*, 141. [[CrossRef](#)]
19. Liu, J.L.; Chen, Z.H.; Huang, H.Y.; Xie, J.X. Microstructure and superelasticity control by rolling and heat treatment in columnar-grained Cu-Al-Mn shape memory alloy. *Mater. Sci. Eng. A* **2017**, *696*, 315–322. [[CrossRef](#)]
20. Dutkiewicz, J.; Kato, H.; Miura, S.; Messerschmidt, U.; Bartsch, M. Structure changes during pseudoelastic deformation of CuAlMn single crystals. *Acta Mater.* **1996**, *44*, 4597–4609. [[CrossRef](#)]
21. Kato, H.; Dutkiewicz, J.; Miura, S. Superelasticity and shape memory effects in Cu-23 at. % Al-7 at. % Mn alloy single crystals. *Acta Metall. Mater.* **1994**, *42*, 1359–1365. [[CrossRef](#)]
22. Ahlers, M. Martensite and equilibrium phases in Cu-Zn and Cu-Zn-Al alloys. *Prog. Mater. Sci.* **1986**, *30*, 135–186. [[CrossRef](#)]
23. Mañosa, L.; Planes, A. Materials with giant mechanocaloric effects: Cooling by strength. *Adv. Mater.* **2017**, *29*, 1603607. [[CrossRef](#)] [[PubMed](#)]
24. Sutou, Y.; Koeda, N.; Omori, T.; Kainuma, R.; Ishida, K. Effect of aging on bainitic and thermally induced martensitic transformations in ductile Cu-Al-Mn-based shape memory alloys. *Acta Mater.* **2009**, *57*, 5748–5758. [[CrossRef](#)]
25. Ossmer, H.; Chluba, C.; Krevet, B.; Quandt, E.; Rohde, M.; Kohl, M. Elastocaloric cooling using shape memory alloy films. *J. Phys. Conf. Ser.* **2013**, *476*, 012138. [[CrossRef](#)]
26. Liu, J.L.; Huang, H.Y.; Xie, J.X. The roles of grain orientation and grain boundary characteristics in the enhanced superelasticity of Cu_{71.8}Al_{17.8}Mn_{10.4} shape memory alloys. *Mater. Des.* **2014**, *64*, 427–433. [[CrossRef](#)]



© 2017 by the authors. Licensee MDPI, Basel, Switzerland. This article is an open access article distributed under the terms and conditions of the Creative Commons Attribution (CC BY) license (<http://creativecommons.org/licenses/by/4.0/>).